Advances in Science and Technology Research Journal

Advances in Science and Technology Research Journal, 2025, 19(6), 301–315
https://doi.org/10.12913/22998624/203278
ISSN 2299-8624, License CC-BY 4.0

Received: 2025.02.22
Accepted: 2025.03.24
Published: 2025.05.01

Optimization of process parameters for compressive strength-to-weight ratio of additively manufactured polyethylene terephthalate glycol

Nareen Hafidh Obaeed[1*], Hind H. Abdulridha[1], Raed R. Shwaish[1], Aqeel S. Bedan[1]

[1] Production Engineering and Metallurgy Department, University of Technology, Iraq, Alsina'a Street, 10066 Baghdad, Iraq
* Corresponding author's e-mail: nareen.h.obaeed@uotechnology.edu.iq

ABSTRACT

Additive manufacturing (AM), particularly the fused deposition modeling (FDM) has become a cornerstone manufacturing technology in the nascent field of 3D printing. The mechanical properties and effective use of material in 3D printed parts are essential for enhancing the potential of AM in industrial and functional applications. This paper explores how core FDM printing process parameters: print temperature, extrusion width, and printing speed affect the compressive strength-to-weight ratio of polyethylene terephthalate glycol (PETG) parts produced via FDM. Based on the Box-Behnken design of response surface methodology (RSM) the influence of these conditions concerning the mechanics and material properties were studied. The results show that a printing temperature of 250 °C provides improved compressive strength as well as decreased weight through strong bonding between layers. Small, extruded widths (0.5 mm) have been found to offer the ideal strength-to-weight ratio while large extruded widths (0.6 mm) greatly enhanced strength by adding weight. A slower printing speed of 30 mm/s promoted greater compressive strength but yielded more dense parts. In the multi-objective desirability optimization, optimal parameters were found in which the printing temperature was 250 °C, the extruded width was 0.5879 mm and the printing speed was 30 mm/s. The results of this study are beneficial for realizing lightweight yet mechanically abundant 3D printing parts while enhancing the field of AM in different industries.

Keywords: fused deposition modeling, polyethylene terephthalate glycol, printing parameters, compressive strength, weight, response surface methodology, Box-Behnken design, desirability analysis.

INTRODUCTION

As a result of increased competition at the worldwide level, the inherent introduction of mass customization of products, and the lengthy cycle time for molding conventional manufacturing processes often required the manufacturing industry to search for different opportunities for new processes that can handle small quantities [1]. It is possible to note that manufacturing technologies have experienced huge changes evolving from the traditional subtractive manufacturing to the advanced additive manufacturing. Traditional processes including machining, casting and forging generally entail material removal or formation by plastic deformation with tools and molds, therefore require considerable material excess, expensive molds, and restricted geometries. These methods are dependable and have stood the test of time, but struggle to address increased call for higher geometries, light-weight and unique designs [2]. In the field of medical, manufacturing, and engineering applications in recent years, 3D printing technology has advanced greatly [3, 4]. Additive manufacturing (AM) or 3D printing is one of the most rapidly advancing and impact technologies that has gained massive trends in manufacturing as it makes it possible to produce the part with the desired geometries that are nearly impossible to produce in the conventional methods of manufacturing while drastically reducing the amount of material used and the cycle time it takes to manufacture a part [5,

6]. AM is a process that incorporates an addition material layer by layer to produce a part from a digital model [7, 8]. Nevertheless, fused deposition modeling (FDM) is one of the most popular technologies of AM because it is relatively cheap, universal, and easy to operate among all available technologies [9]. FDM can be best described as a welding process, in which layers of thermoplastic are melted and then solidified one atop the other, and the layers are bonded together similarly to how it happens in a welding process [10, 11]. Initially developed for rapid prototyping, FDM has become one of the reliable methods for fabricating functional parts and complex geometries with desirable properties that can be used in diverse industrial and biomedical applications [12, 13]. Nonetheless, the mechanical properties and weight of the elements printed by FDM largely depend on the process parameters, and thus the optimization is crucial for high-performance applications [14].

Polyethylene terephthalate glycol-modified also known as polyethylene terephthalate glycol (PETG) is a widely used 3D printing material that has grown in popularity for its use in additive manufacturing because it has strength, chemical resistance, and ease of processing. However, PETG has unique compressive properties when it is processed by FDM making it suitable for use in the biomedical engineering industry, automotive industry, and many others. Due to its toughness and resistance to shock it is ideal for creating functional prototypes and end-use parts [15].

The literature has shown various studies regarding the impact of process parameters on compressive properties, for instance, Hassan et al. [16] (2020) focused on manufacturing of bone scaffold using polyethylene terephthalate glycol (PETG), a glycol-modified PET. In this study, PETG scaffolds with pore sizes of 300, 350, and 450 μm were prepared with the help of a continuous filament-based extrusion 3D printing system. PETG scaffolds with pore size of 300μm were found to have higher values for mechanical properties than polycaprolactone (PCL) scaffolds, thus it was concluded that PETG scaffolds provided greater cell attachment and proliferation.

Petersmann et al. [17] (2020) examined the mechanical properties of polymers that can be 3D printed; these include polylactide (PLA), poly(vinylidene fluoride) (PVDF), polyetheretherketone (PEEK), glycol-modified poly(ethylene terephthalate), poly(methyl methacrylate) (PMMA), and polypropylene (PP) tested at preferred crosshead speed; dynamic mechanical analyses. The analysis proved that the physical characteristics of these materials do not vary with temperature fluctuations within the body of a human. However, in the progressively increasing body temperature, both PVDF and PP revealed a reduction in their stiffness. The dependence of stiffness on the strain rate also rises from PLA to PP, PEEK, PETG, PMMA and PVDF. To assess the processability of the investigated materials, their filling density was also ranked. Such information can be useful in choosing medical applications and developing implants based on 3D printing.

Özen et al. [18] (2021) investigated the behavior of structures fabricated by additive manufacturing with emphasis on fused deposition modeling technique. ASTM D3039 and ISO 527-2 standards are used to compare four different Ptensile test specimens for PETG. Specimen geometries are analyzed using the finite element method (FEM). Tests for uniaxial tensile strength are performed on specimens produced employing the various 3D printing slicing techniques. The effect of slicer parameters on failure position is highlighted in the study and simple formulation developed for quantifying the mechanical properties of parts made using 3D printing. Mahesh et al. [19] (2021) outlined the mechanical properties of PETG composite filaments produced by 3D printing without post-processing. The filaments are prototyped using fused deposition modeling and their tensile, compression, flexural, impact, and hardness performances evaluated. While organically modified montmorillonite nanoclay has a positive impact on the properties of the composites, short carbon fibers has little influence because of the existence of interstitial voids as well as weak matrix fiber adhesion. These composites may be applied in aerospace applications, automotive applications, orthotic, and prosthetic uses. The study also provides other potential process parameter changes and post-processing treatments which can give better properties.

Valvez et al. [20] (2022) focused on static properties, creep, and stress relaxation on PETG / carbon and Kevlar fiber composites. It was realized that the yield compressive strength reduced in both the composites but to a higher extent in the presence of clay compared to the neat polymer. The compressive displacement was also reduced by 20.4% and 46.3% respectively. The enhancement to the compressive modulus was 12.4% when incorporating

carbon fibres in the PETG matrix while it was a reduction of 39.6% when incorporating Kevlar fibres. Stress relaxation behavior revealed the reduction of compressive stresses over time for neat PETG while creep response favors increasing of compressive displacement. But when the fibers were incorporated in the polymer, greater stress relaxations and displacements were achieved. Raffic et al. [21] (2022) focused on optimizing four different FDM parameters in three levels: layer height, infill density, shell thickness, and raster angle all have been varied for the purpose of decreasing the printing time, the weight of the part, and improving the flexural modulus of PET-G material modified using Polyethylene Terepthalate-glycol. Mono optimization is performed using Taguchi's L9Orthogonal Array (OA) and multi response optimization is performed using grey relational analysis (GRA) and technique of order preference similar to ideal solution (TOPSIS). Both Shanon entropy and CRITIC methods provide the weightages of the responses. In general, the results suggest that infill density correlates strongest with the output assessed parameters, where A2B1C1D2 is the best parameter setting. There are confirmation trials to prove that the settings found optimized are optimum.

Vijayasankar and Falguni [22] (2023) concentrated on enhancing the print setting of PETG silk fibroin (PETG-SF) composite material in order to 3D-print medical products such as scaffolds, implants, prosthetics, and orthotics. Optimization of process parameters of PETG-SF composites was done by single as well as multi-objective optimization. It was also shown that the variation of layer height and print temperature had the greatest influence on maximum dimensional accuracy, yield load, and minimum porosity. Analyzing multiple objectives, it was found that low temperature and low speed with small layer height are the optimal printing parameters for minimizing porosity, maximizing the yield load, ad ad aperture. These settings were then used to print a generic organic shape as the result for the formulation of patient specific anatomically conforming prosthesis and implants. Vijayakumar et al. [23] (2023) aimed at implementing hexagonal lattice shell structure as outer wall in PTTG/carbon fiber composite. Samples are prepared with fused filament fabrication TPP method and basic printing parameters. L9 orthogonal array response is employed with respect to compressive strength and dimensional errors. Taguchi and Analysis of Variance techniques are employed to identify appropriate conditions for the printing solution. The highest level of compressive strength is achieved at the parameters such as nozzle temperature of 220 °C, layer height of 0.1mm, infill density of 100% and printing speed of 20 mm/s.

Petousis et al. [24] (2023) examined how the compression loading rate of four thermoplastic polymers behaves in the context of MEX 3D printing. PC, PETG, PMMA, and TPU materials were chosen in raw powders and underwent the melt extrusion process and then 3D printed. Compressive strength, yield stress, modulus of elasticity, material toughness, and maximum compressive sensitivity index were reported. As the strain rate increased, both PMMA and TPU rise while the PC has the highest rate of strain rate sensitivity. The results of the calculations may be used in industrial engineering as design optimization input parameters for different polymeric materials. Patil et al. [25] (2024) aimed at determining the effects of infill patterns and percentages on the compressive strength of the carbon fiber-reinforced PETG parts produced by FDM. From the research process which utilizes response surface methodology, it is shown that strength is improved by an increase in the infill density. More precisely, a 80% infill density with a tri-hexagon pattern has 39.16 MPa of compressive strength. The studies are useful for developing recommendations on improving the quality of PETG parts, especially in automobiles and aerospace applications, which require high-performance polymers.

This study fills a vital gap in FDM-based PETG research by optimizing the compressive strength-to-weight ratio which earlier research has neglected. The research examines the combined effects of printing temperature and extrusion width as well as printing speed through its comprehensive evaluation of all parameters. A multi-objective desirability optimization method allows the production of light yet durable 3D-printed components by finding their best strength-to-weight ratio, to be suitable for a wider variety of biomedical engineering and industrial applications.

METHODOLOGY

Materials and methods

PETG was selected based on its good mechanical properties such as high tensile strength, resistance to impact, and excellent stability

of dimensions. So, PETG has been widely employed in a wide range of FDM applications requiring durability and moderate flexibility, hence; it is a good candidate for compression testing. To avoid degradation induced by the moisturizing, before it was used the filament was kept in a sealed container with desiccant material.

The compressive samples were designed by SOLIDWORKS software with specified dimensions Φ 12.7 mm and 25.4 mm for diameter and length respectively followed by the ASTM D695 standards and then converted to stereolithography (STL) file format, as shown in Figure 1, then transferred to slicing software for horizontal slicing into thin layers with two-dimensional contour information for the process plan to determine the tool path controlling the FFF machine hardware. The Ultimaker Cura program, version 5.6.0, generated STL files sliced into machine-readable G-code. Cura software functions as a virtual slicing system that divides CAD models while generating support features and establishing print parameter values before positioning the model for the printer surface. PETG compression test specimens were manufactured in vertical orientation via FDM Creality Ender 3 Pro 3D printer machine of 220 × 220 × 250 mm print volume with 0.4 mm nozzle diameter as depicted in Figure 2. A consistent vertical printing orientation was maintained throughout all the samples to achieve standardized mechanical performance along with eliminating FDM-printed anisotropic effects. Layers stack in a perpendicular position relative to the build plate surface because the Z-axis serves as the primary direction for layer deposition. A constant printing direction resulted in a standardized analysis of the relationship between printing temperature, extrusion width and speed and compressive strength-to-weight ratio. This study utilized CREALITY (CR series) PETG filament with a diameter of 1.75 mm was used for manufacturing standard compressive specimens.

The design of experiments (DoE), namely the Box–Behnken design is used to establish a robust

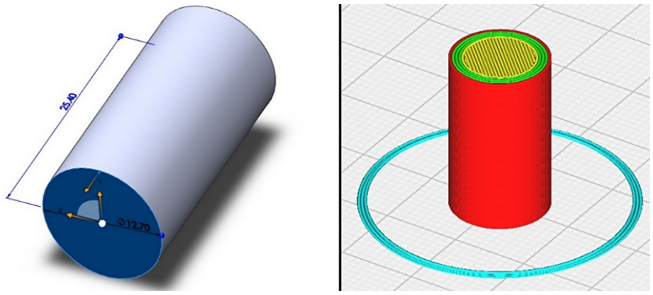

Figure 1. CAD and sliced models for standard compression specimens (dimensions in mm)

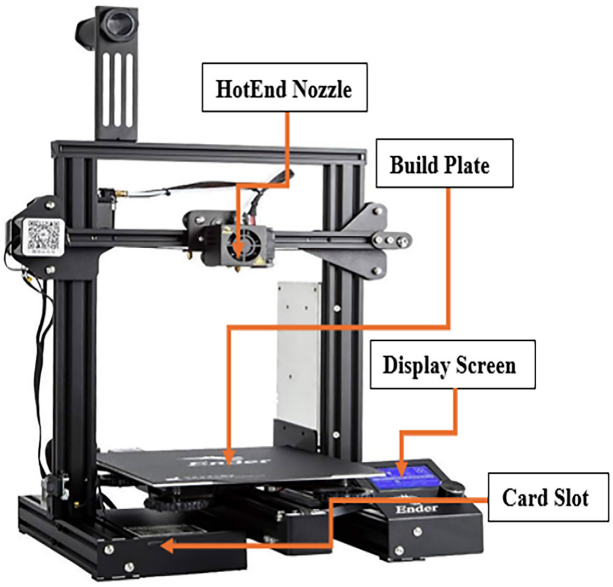

Figure 2. Creality Ender-3 Pro that is utilized in this study

and systematic methodology for determining optimal machining conditions in the manufacturing process. The Box-Behnken design functions as part of response surface methodology (RSM) to optimize experimental data. As a second-order rotatable design Box-Behnken avoids corner points of the cube through selective factor combinations therefore providing better efficiency and cost management than full factorial designs. The methodology uses its design to detect variable connections in non-linear dimensions while decreasing experimental requirements. The FDM process parameters were divided into two classifications constant and variable. Three variables of manufacturing parameters (extruded width, printing speed, and printing temperature) each at three levels are illustrated in Table 1. The extruded width refers to the actual width of each deposited filament track emerges directly from the nozzle during printing operations. The constant parameters of all printed samples with their values are illustrated in Table 2.

The manufactured standard samples followed the experimental design of Box–Behnken design. Fifteen test samples with dimensions were 3D-printed by the design of the experiment. The overall view of the printed samples is presented in Figure 3.

Desirability analysis method

Desirability Analysis (DA) is a statistical means employed in the assessment and enhancement of more than one response or characteristic. It is most used in industries like manufacturing, process optimization, and product designing, where it helps to facilitate better decisions and performance. DA offers a systematic approach to evaluating the desirability of certain outcomes and finding the right parameters combination to achieve multiple objectives [26].

In this method, each objective is modeled by a desirability function that maps objective values to the interval [0, 1]. This scale shows the desirability of each level and is summed into a desirability function for each combination of the input parameters. The desirability value of D_i equal to 1 suggests that the response has been fine-tuned, while the desirability value of 0 of D_i shows that the response is out of acceptable range. The desirability values are obtained according to the "lower-the-better" or "higher-the-better" criterion depending on whether the goal is to minimize or maximize the response variable. Specifically, the desirability value D_i reaches 0 when the response is above a certain value and equals 1 when it is below this value. It is important to note that the value of D_i will always be between zero and one [27]. For "lower is better" requirements, the desirability function is defined by Equation 1, and the overall desirability (D_o) is calculated using Equation 2, which combines individual desirability values and their respective weights.

Lower-The-Better:

$$D_i = \begin{cases} 1 \; if \; y \le L, \\ \left(\frac{U-y}{U-L}\right)^r \; if \; L < y < U, \\ 0 \; if \; y \ge U, \end{cases} \tag{1}$$

$$D_o = (D_1{}^{w_1} * D_2{}^{w_2} \ldots\ldots D_n{}^{w_n})^{(1/\Sigma w_i)} \tag{2}$$

where: Di is the desirability value for the response, L is the lower or target level of the response below which the response is completely favorable, U is the upper limit of response which can be considered unacceptable, r is a weight factor that decides how important it is to be close to the lower target (L), D_1, D_2, …, *and* D_m represent the individual desirability values for m responses, and w_1, w_2, …, w_m represent weights assigned to the importance of each response.

Table 2. The constant parameters with their values

Constant parameters	Value
Sample dimension	Φ12.7 × 25.4 mm
Layer height	0.2 mm
Wall thickness	1.2 mm
Infill density	75%
Infill pattern	Cubic
Building plate temperature	80 °C
Nozzle diameter	0.4 mm

Table 1. FDM PETG 3D printing process parameters and their levels

Process parameters	Symbol	Unit	Level 1	Level 2	Level 3
Printing temperature	A	ºC	230	240	250
Extruded width	B	mm	0.4	0.5	0.6
Printing speed	C	mm/s	30	45	60

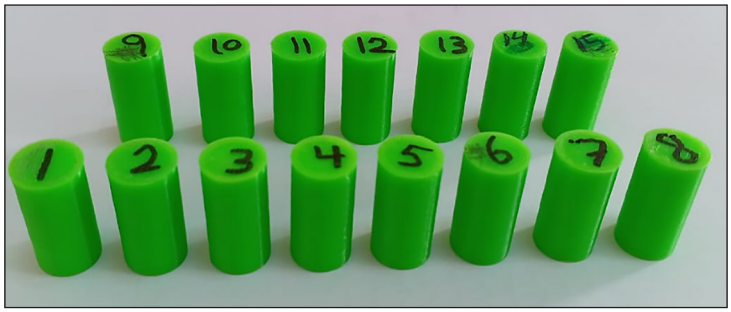

Figure 3. 3D printed PETG samples for compressive strength tests

Testing

The standard samples were examined for weight, and compressive strength after being fabricated based on the design of experiments by changing the input process parameters, then were analyzed to spot the best level for taken variables and which factor has a statistically significant impact on the specific response.

The weight of the samples was determined by using a digital weight instrument type DENVER with a precision of four decimal places to increase the reliability and repeatability of the measurement process while evaluating the weight characteristics of the fabricated parts as depicted in Figure 4. Whereas, the compression test was performed by compression testing utilizing a computer-controlled electronic universal testing machine type WDW-200E with a load cell of 200 kN capacity to test all the manufacturing samples, as shown in Figure 5. The standard samples were compressed at a rate of 2 mm/min. These two tests were conducted in the Laboratories of the Production Engineering and Metallurgy Department at the University of Technology/ Iraq. The compressive strength of each test specimen was estimated based on Equation 3:

$$\sigma = \frac{F}{A} \tag{3}$$

where: σ – compression stress in N/mm², F – force in N, A – cross sectional area of the fabricated part in mm².

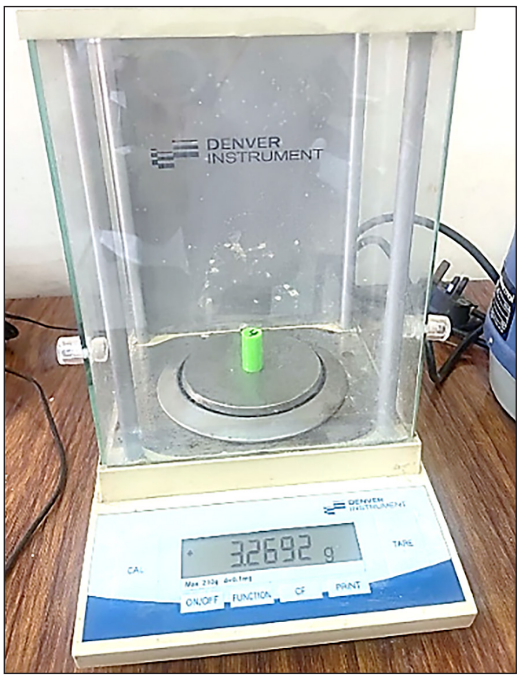

Figure 4. Weight instrument used in this study

RESULTS AND DISCUSSION

The fifteen PETG compressive standard samples after performed testing are illustrated in Table 3.

Microscopic images referred to the samples surface topography using an optical microscope type OPTIKA after the compression test depicted the deformation visualization, as shown in Figure 6. The optical microscope images display how the lateral PETG specimen surface deformed following compression testing. Under compressive loading the material shows different layer structures and bonding patterns as well as surface irregularities according to the displayed pictures. Print parameters appear to affect mechanical performance based on the visible shear deformations along with discontinuities found between layers.

The results from the residual analysis of both weight and compressive strength indicate key statistical assumptions are met for both weight and compressive strength, validating the reliability of the model as demonstrated in Figures 7 and 8. The normal probability plot of residuals has residuals close to the reference line indicating approximate normality and residuals in the versus fits plots are scattered randomly around zero, indicating little

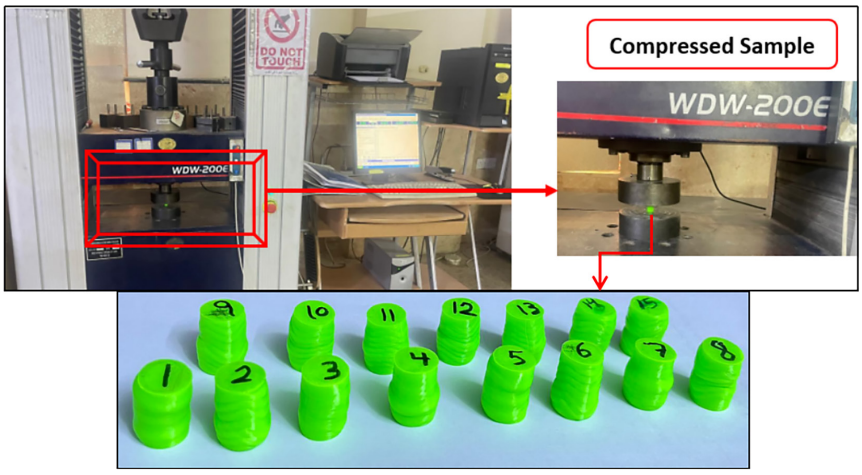

Figure 5. Compression testing setup utilization in this study

Table 3. The weight and compressive strength for PETG specimens

No. of run	Printing temperature (ºC)	Extruded width (mm)	Printing speed (mm/s)	Weight (g)	Compressive strength (MPa)
1	240	0.4	30	3.3705	34.43
2	240	0.6	30	3.3301	41.08
3	240	0.4	60	3.2904	36.81
4	240	0.6	60	3.4692	36.75
5	230	0.4	45	3.2592	39.13
6	230	0.6	45	3.2811	36.96
7	250	0.4	45	3.2909	34.99
8	250	0.6	45	3.3187	42.88
9	230	0.5	30	3.2289	35.89
10	230	0.5	60	3.2274	34.66
11	250	0.5	30	3.2671	35.15
12	250	0.5	60	3.2699	32.78
13	240	0.5	45	3.2535	35.29
14	240	0.5	45	3.2818	35.25
15	240	0.5	45	3.2822	34.98

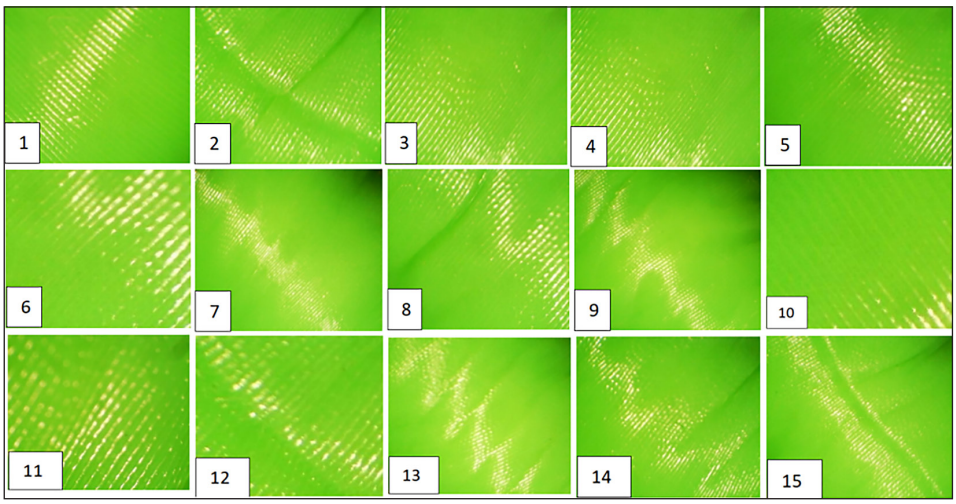

Figure 6. Optical microscope images depicted the topography belong to lateral PETG surface after compression test

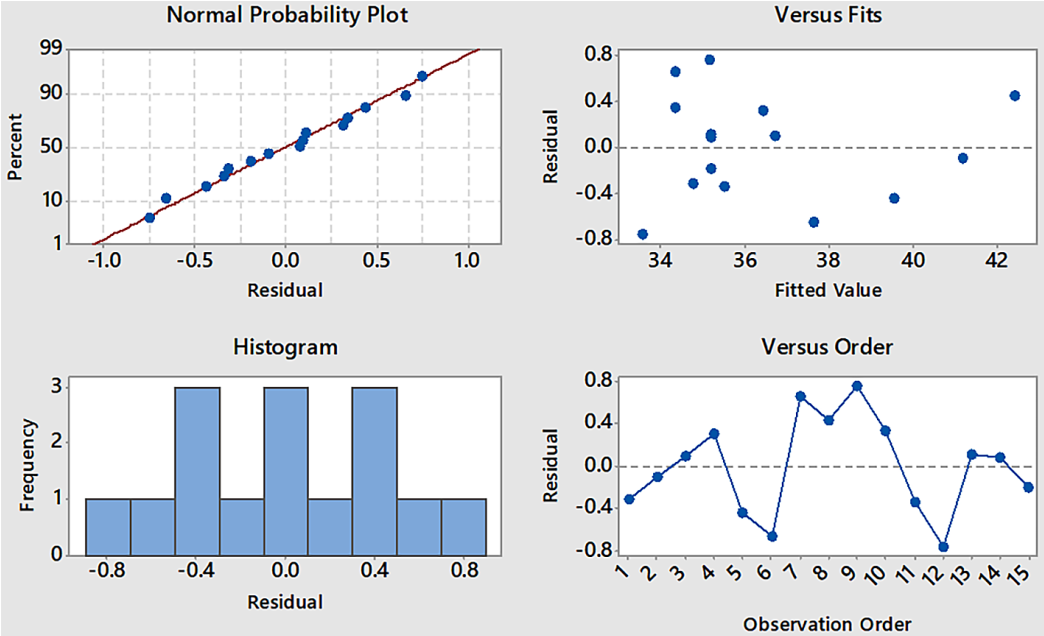

Figure 7. Residual plots for compressive strength

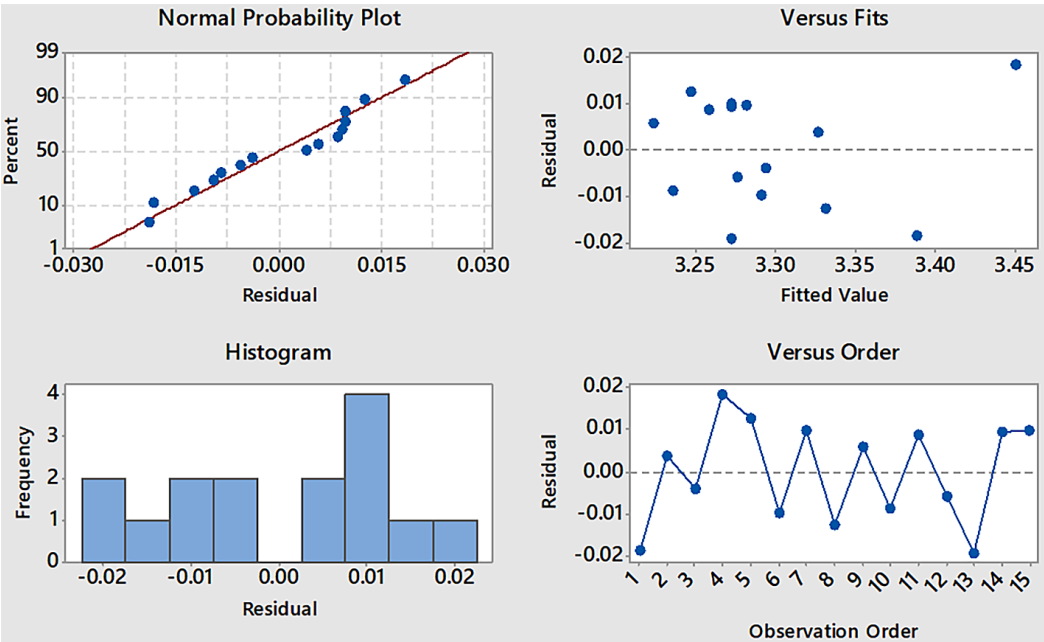

Figure 8. Residual plots for weight response

evidence of nonlinearity or heteroscedasticity in the fit. Residual distribution is found symmetric in the histogram, which does not show any autocorrelation in the versus order plot, therefore residuals are independent. For compressive strength, the normal probability plot of the residuals indicates that residuals are approximately normally distributed. The versus fit plot indicates a random scatter around zero and a good fit with minor heteroscedasticity at higher fitted values. The histogram indicates a rough symmetric distribution, and it appears there is no temporal bias in the versus-order plot. These models have been validated for both responses, and the effects of printing temperature, extruded width, and printing speed on the weight and compressive strength of PETG specimens are both predictable and statistically robust.

The interpretation of the main effects and interaction plots offers important information about the effect of printing temperature, extruded width,

and printing speed on the compressive strength and weight of 3D PETG parts. Figure 9 shows the main effects plot that the effect of printing temperature is slightly positive on the compressive strength when printed at temperatures up to 250 °C for printed parts while for the extruded width, there is a parabolic relationship whereby the printed parts with the highest compressive strength have an extruded width of 0.6 mm. The overall trend observed when analyzing the effect of printing speed is negative, where higher printing speed decreases the compressive strength of printed parts. The compressive strength of a structure depends on the internal pore size that results directly from extrusion width combined with processing speed. Material deposition through wider extrusion increases strength but leads to more substantial weight addition. Prints operated at slower speeds help layers to fuse more efficiently thus creating fewer voids and strengthening the structure. These control parameters determine the internal pore development process which affects both pressure response and the total mechanical abilities of the printed product.

While the weight study concerning the printing parameters is depicted in Figure 10, there is a trade-off between PETG print material and the mechanical strength of the optimized 3D printed parts. The weight is observed to rise mildly with the printing temperature of up to 240 °C but declines at 250 °C, demonstrating improved material densification. Same with the case of extruded width, weight increases parabolically with the thickness, with the minimum at 0.5 mm and a sharp rise at 0.6 mm owing to an increased quantity of material used. Similarly, the weight exhibits an inverted U-shape relationship with the printing speed at which the

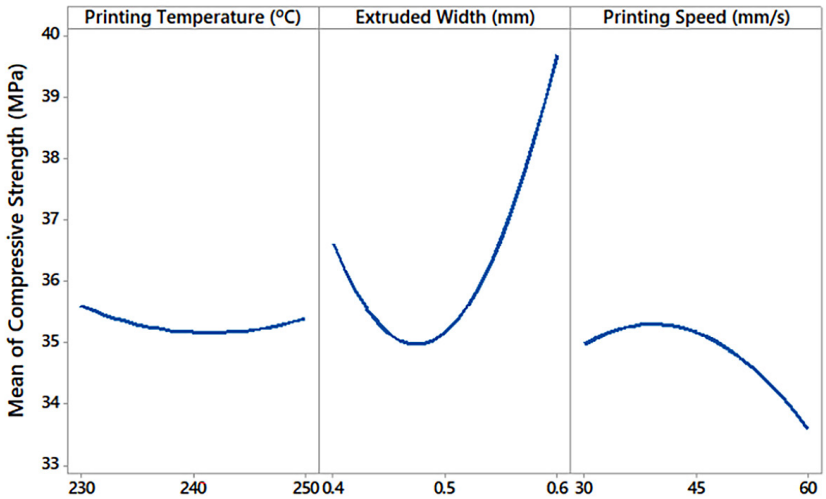

Figure 9. Main effect plot for compressive strength response

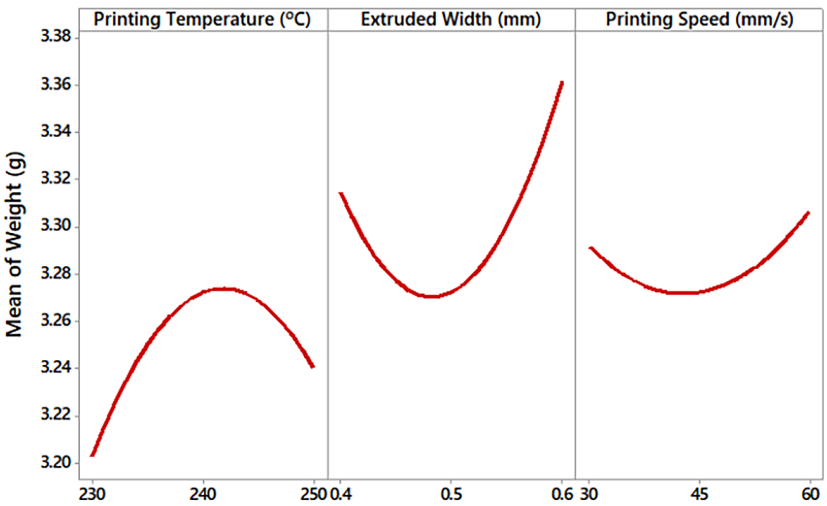

Figure 10. Main effect plot for weight response

minimum value is at 45 mm/s. Comparing these results with the analysis of compressive strength, a trade-off emerges: the parameters that improve compressive strength influence the weight likewise; for instance, broader extrusion widths (0.6 mm) and reduced printing speed (30 mm/s). However, even at printing temperatures of 250 °C, a combination that enhances both compressive strength and weight reduction occurs.

Table 4 demonstrates the ANOVA results that give a detailed analysis of the parameters that significantly influenced the compressive strength (MPa) and weight (g). For compressive strength, the model accounts for 97.11% of the

Table 4. Analysis of variance for compressive strength and weight responses

Analysis of variance for compressive strength (MPa)						
Source	DF	Adj SS	Adj MS	F-Value	P-Value	% contribution
Model	9	97.348	10.8164	18.66	0.002	97.109
Linear	3	22.874	7.6246	13.16	0.008	22.818
A	1	0.085	0.0849	0.15	0.718	0.085
B	1	18.936	18.9359	32.67	0.002	18.890
C	1	3.853	3.8531	6.65	0.050	3.844
Square	3	37.554	12.5181	21.60	0.003	37.462
A*A	1	0.408	0.4077	0.70	0.440	0.407
B*B	1	32.796	32.7956	56.59	0.001	32.716
C*C	1	2.910	2.9096	5.02	0.075	2.903
2-way interaction	3	36.920	12.3066	21.24	0.003	36.829
A*B	1	25.296	25.2959	43.65	0.001	25.234
A*C	1	0.324	0.3243	0.56	0.488	0.323
B*C	1	11.300	11.2997	19.50	0.007	11.272
Error	5	2.898	0.5795			2.891
Lack-of-fit	3	2.841	0.9471	33.67	0.029	2.834
Pure error	2	0.056	0.0281			0.056
Total	14	100.246				100.000
Analysis of variance for weight (g)						
Source	DF	Adj SS	Adj MS	F-Value	P-Value	% contribution
Model	9	0.049802	0.005534	14.13	0.005	96.219
Linear	3	0.007690	0.002563	6.55	0.035	14.857
A	1	0.002812	0.002812	7.18	0.044	5.433
B	1	0.004423	0.004423	11.30	0.020	8.545
C	1	0.000455	0.000455	1.16	0.330	0.879
Square	3	0.030086	0.010029	25.62	0.002	58.127
A*A	1	0.009557	0.009557	24.41	0.004	18.464
B*B	1	0.016011	0.016011	40.90	0.001	30.934
C*C	1	0.002632	0.002632	6.72	0.049	5.085
2-way interaction	3	0.012025	0.004008	10.24	0.014	23.233
A*B	1	0.000009	0.000009	0.02	0.887	0.017
A*C	1	0.000005	0.000005	0.01	0.918	0.010
B*C	1	0.012012	0.012012	30.68	0.003	23.208
Error	5	0.001957	0.000391			3.781
Lack-of-fit	3	0.001416	0.000472	1.74	0.385	2.736
Pure error	2	0.000542	0.000271			1.047
Total	14	0.051759				100.000

Note: A – printing temperature (°C), B – extruded width (mm), and C - printing speed (mm/s).

total variation explicated by R-sq, whereby linear terms accounted for 22.82% of the total variation, quadratic terms accounted for 37.46%, while two-way interactions accounted for 36.83%. Among these parameters, extruded width is found to be significant with linear and quadratic contributions of 0.002 and 0.001, respectively. The compressive strength of a material depends on extruded width because this parameter controls the material deposition per layer which impacts both bonding strength between layers and structural stability. The significant interactions between print temperature with extruded width (25.23%) and extruded width with the print speed (11.27%) imply that extruded width has a great influence on the compressive strength. However, lack-of-fit is highly significant (P = 0.029), indicating a need for improvement of the model or to add more terms to account for the total variability of the data.

Similarly, for weight, the model fits are equal to 96.22% (R-sq), and the quadratic terms contributed the most with 58.13%. Again, extruded width is found to be most influential, with the quadratic term contributing 30.93% of the variation, while print speed does not impact weight because it controls material density rather than altering the amount of material used according to established layer settings. The effects of combined interaction between extruded width and printing speed are also considerable (23.21%). In contrast to the compressive strength model, the result of the weight model does not show any lack of fit (P = 0.385), which means that the models have good fitness towards the collected data. Both the models present a good fit and adherence to the given data, while the compressive strength model suggests overfitting and a high lack-of-fit, which means better opportunities for improvement in the prediction as well as accuracy in the model.

The interaction plots presented in Figures 11 and 12 indicate the presence of such relationships between these parameters. The printing parameters interactions suggest that the relationships between the process settings and the final part properties printing namely the compressive strength and weight of the 3D printed part involve multifaceted interactions. Regarding printing temperature and extruded width, it was observed that printing at high temperature (250 °C) and medium extruded width (0.5 mm) produces material with comparatively low weight but possessing a moderate compressive strength as compared to the one produced at 0.6 mm width which has maximum strength but highest weight. The relationship between printing temperature and printing speed shows lower speeds (30 mm/s) are beneficial to increase the compressive strength across the temperature range with negligible effect on weight. On the other hand, higher speeds such as 60 mm/s lead the bonding to be poor hence leading to a reduction in the strength. Likewise, the results of extruded width and print speed also reveal that wider extruded width (0.6 mm) provides maximum compressive strength, particularly at reduced speeds; moderate width minimizes weight on the other hand is rather insensitive to speed. However, the optimal setting for the parameter to get a maximum value of compressive strength per unit weight of the part can be summarized as follows: a high value of the printing

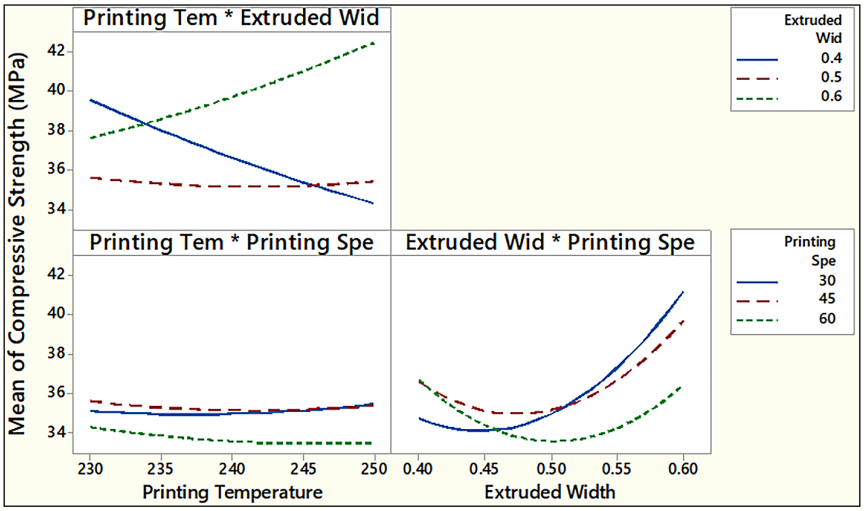

Figure 11. Effect of parameters levels on compressive strength

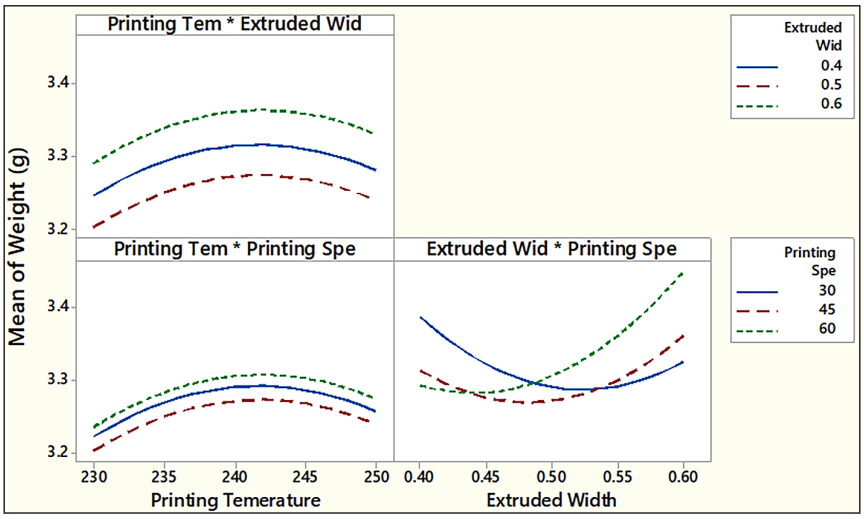

Figure 12. Effect of parameters levels on weight response

temperature (250 °C), a medium value of the extruded width (0.5 mm), and a moderate value of the printing speed (45 mm/s).

RSM predictive modelling

Response Surface Methodology is a powerful statistical tool for modeling and optimizing processes, especially for studying the relation between many of the input parameters and a single or multiple output factor. Table 5 presents a comparison between the experimental results and the values predicted by RSM for the mechanical properties and physical properties of PETG standard specimens based on the quadratic regression models of Equations 4 and 5. This comparison will be used to assess the degree of precision and reliability of the prediction models constructed for this research. The predicted ranges of compressive and weight strength, which cover RSM results, are provided for given ranges of printing temperature, extruded width, and printing speed. The compressive strength and weight are shown in the Table 5 under various combinations of the parameters that were examined. RSM fits the mathematical model to experimental data, extracting interaction effects and curvature of the response surface

Table 5. Comparison of experimental and predicted results of compressive strength and weight

No. of Exp.	Printing temperature (ºC)	Extruded width (mm)	Printing speed (mm/s)	Compressive strength (MPa)	Predicted compressive strength (MPa)	Error (%)	Weight (g)	Predicted weight (g)	Error (%)
1	240	0.4	30	34.43	34.74	0.90	3.3705	3.3888	0.54
2	240	0.6	30	41.08	41.18	0.24	3.3301	3.3262	0.11
3	240	0.4	60	36.81	36.72	0.24	3.2904	3.2943	0.11
4	240	0.6	60	36.75	36.43	0.87	3.4692	3.4509	0.52
5	230	0.4	45	39.13	39.57	1.12	3.2592	3.2467	0.38
6	230	0.6	45	36.96	37.62	1.78	3.2811	3.2908	0.29
7	250	0.4	45	34.99	34.33	1.88	3.2909	3.2812	0.29
8	250	0.6	45	42.88	42.44	1.02	3.3187	3.3312	0.37
9	230	0.5	30	35.89	35.13	2.11	3.2289	3.2231	0.17
10	230	0.5	60	34.66	34.31	1.01	3.2274	3.2360	0.26
11	250	0.5	30	35.15	35.49	0.96	3.2671	3.2585	0.26
12	250	0.5	60	32.78	33.54	2.31	3.2699	3.2757	0.17
13	240	0.5	45	35.29	35.18	0.31	3.2535	3.2725	0.58
14	240	0.5	45	35.26	35.18	0.22	3.2818	3.2725	0.28
15	240	0.5	45	34.98	35.18	0.57	3.2822	3.2725	0.29

thus providing precise predictions. The predictive models agreed with experimental results by producing slightly varying predictions which shows the models deliver trustworthy estimates for the examined parameter range.

$$\begin{gathered} Compressive\ Strength\ [MPa] = 546 - 2.78 \times \\ \times A - 836 \times B + 1.325 \times C + 0.00332 \times A^2 + \\ + 298 \times B^2 - 0.00395 \times C^2 + \\ + 2.515 \times A \times B - 0.0019 \times A \times \\ \times C - 1.12 \times B \times C \end{gathered} \tag{4}$$

$$\begin{gathered} Weight\ [g] = -23.66 + 0.245 \times A - 8.35 \times B - \\ - 1.325 \times C - 0.000509 \times A^2 + 6.59 \times B^2 - \\ + 0.000119 \times C^2 + 0.00148 \times A \times B + \\ + 0.000007 \times A \times C + 0.03653 \times B \times C \end{gathered} \tag{5}$$

Multi-objective desirability optimization

For compressive strength, an optimized value of 42.8366 is achieved, with near-perfect desirability equal to 0.9958, and for weight 3.2831, the best desirability of 0.76957 is achieved. The optimal conditions of printing temperature are 250 °C (at the high level), an extruded width of 0.5879 mm (near the mild level of the parameter), and a printing speed of 30 mm/s (at the lower level). Results demonstrate the strong influence of printing temperature on compressive strength, along with the extruded width and printing speed to fine-tune the desired trade-off. The results confirm the use of the desirability function in the framework of balanced optimization of competing objectives and the robust parameter set. With this approach, 3D printing settings can be effectively tailored for compression strength and weight requirements that are application-dependent. Optimization is a key issue in engineering and manufacturing because it enables finding the best systematic solution for a combination of input parameters to attain specific output. The multi-objective optimization of compressive strength and weight were carried out using desirability-based analysis to determine the optimal values of the input parameters: printing speed, extruded width, and printing temperature as depicted in Figure 13. To optimize this by maximizing the compressive strength and minimizing the weight, a composite desirability of 0.8754 was found, indicating a strong balance between the two objectives.

CONCLUSIONS

This work aimed at identifying process parameters for FDM fabrication process affording enhanced compressive strength and light weight of the PETG material. Subsequently, based on response surface methodology applying a Box–Behnken design, simulation models

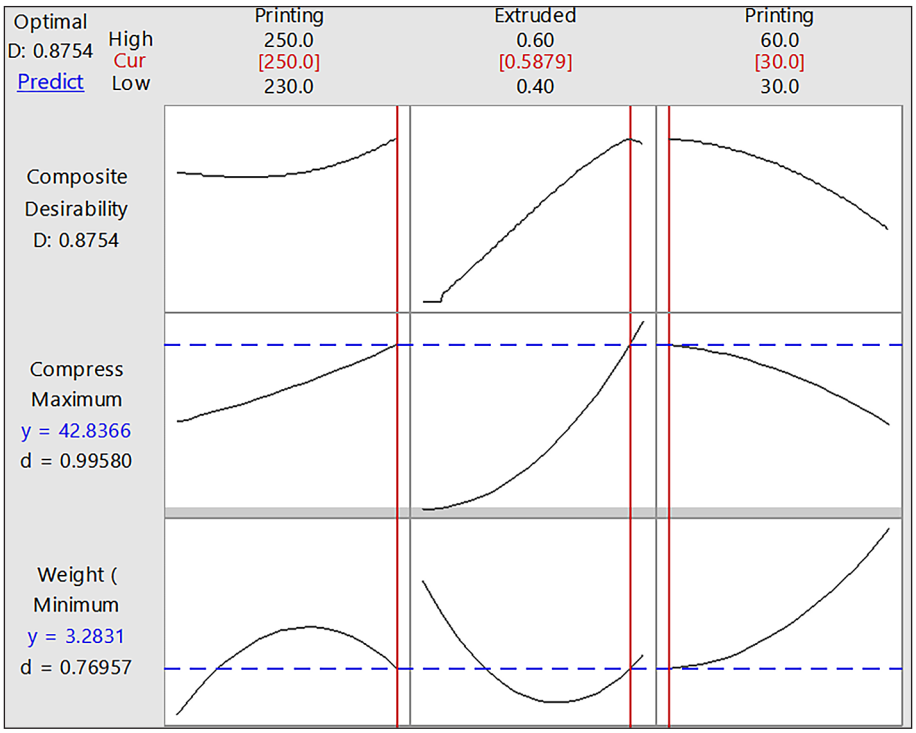

Figure 13. Multi-objective desirability optimization of compressive strength and weight responses

were established and the impact of various major process parameters, including the printing temperature, printing width, and printing speed, on the compressive strength and weight of the printed PETG parts were assessed. The mechanical strength was determined through the compression tests while weight measurements were employed to evaluate material utilization and lightweight capability. The primary findings of the study are as follows:

1. Experimental results demonstrated that the highest compressive strength of 42.88 MPa was achieved with a printing temperature of 250 °C, extruded width of 0.6 mm, and a printing speed of 45 mm/s. These settings produced components with exceptional mechanical performance under compressive loading.
2. To minimize weight while maintaining adequate compressive strength, the optimal configuration was determined to include a printing temperature of 230 °C, extruded width of 0.5 mm, and a printing speed of 60 mm/s. This combination resulted in a significant reduction in material usage, supporting the lightweight design without severely compromising mechanical properties.
3. The ANOVA analysis also shows that there is a strong correlation between extruded width (B) and both the compressive strength and the weight and it contributes 32.71% to variances in the compressive strength and 30.93% of the weight reduction. Furthermore, the combined effects of the printing temperature (A), and the extruded width (A*B) are significant in achieving an optimal level of compressive strength whereas, the combined effects of the extruded width (B), and the printing speed (C) is important to get the minimum weight.
4. For maximum compressive strength, the optimal parameters were a printing temperature of 230 °C, extruded width of 0.6 mm, and a printing speed of 45 mm/s, while to achieve the minimum weight with acceptable compressive strength, the ideal settings included a printing temperature of 240 °C, extruded width of 0.6 mm, and a printing.
5. A desirability analysis was used to determine the optimal parameters that would produce a high compressive strength while on the same time minimizing the weight. The key parameters that provided the highest print quality and performance indicated by maximum compressive strength and minimum component weight were printing temperature = 250 °C; extruded width = 0.5879 mm; and printing speed = 30 mm/s which resulted in a compressive strength of 42.84 MPa and a weight of 3.2831 g showing that the components were both strong and lightweight.

This research demonstrates that response surface methodology is helpful in optimizing FDM parameters for the improvement of PETG mechanical properties in terms of compressive strength and the applicability of FDM parts in lightweight structures. Further studies might focus on other settings like nozzle temperature or other more infill patterns in order to enhance the process. Furthermore, the incorporation of other composite materials or hybrid structures may lead to better performance, thus opening up new possibilities for the use of FDM for further enhanced applications in aerospace, automotive and structural industries.

REFERENCES

1. Hsueh MH, Lai CJ, Wang SH, Zeng YS, Hsieh CH, Pan CY, Huang WC. Effect of printing parameters on the thermal and mechanical properties of 3d-printed pla and petg, using fused deposition modeling. Polymers. 2021 May 27; 13(11): 1758.
2. Mohammed AR, Jawad WK. Experimental and theoretical investigations of octagonal shapes using multi-stage deep drawing process. InAIP Conference Proceedings 2023 Dec 22; 2977(1). AIP Publishing.
3. Obaeed NH and Hamdan WK. Cranioplasty materials for human skull rehabilitation. In Advancements in Sustainability Systems, R. A. Hussain H. Al-Kayiem, Hasanain A. Abdul Wahhab, And Jessam, Ed., New York: Nova Science Publishers, 2024; 123–140.
4. Chunhua S, Guangqing S. Application and development of 3D printing in medical field. Modern Mechanical Engineering. 2020 Aug 10; 10(3): 25–33.
5. Godina R, Ribeiro I, Matos F, T. Ferreira B, Carvalho H, Peças P. Impact assessment of additive manufacturing on sustainable business models in industry 4.0 context. Sustainability. 2020 Aug 30; 12(17): 7066.
6. Mansor KK, Shabeeb AH, Hussein EA, Abbas TF, Bedan AS. A Statistical Investigation and Prediction of the Effect of FDM Variables on Flexural Stress of PLA Prints. Tikrit Journal of Engineering Sciences. 2024 Jul 2; 31(3): 10–7.
7. Obaeed NH, Hamdan WK. Reconstruction and evaluation of 3D Printing PMMA cranioplasty implants. International Journal on Interactive Design

and Manufacturing (IJIDeM). 2024 Aug; 18(6): 4233–45.

8. Abdullah MA, Abbas TF. Numerical developing the internet of things to remotely monitor the performance of a three dimensions printer for free-form surface. Journal of Engineering Science and Technology. 2023 Dec; 18(6): 2809–22.
9. Ning F, Cong W, Qiu J, Wei J, Wang S. Additive manufacturing of carbon fiber reinforced thermoplastic composites using fused deposition modeling. Composites Part B: Engineering. 2015 Oct 1; 80: 369–78.
10. Farajian M. Additive manufacturing processes and performance. Welding in the World. 2023 Apr; 67(4): 831–2.
11. Dauod DS, Mohammed MS, Aziz IA, Abbas AS. Mechanical vibration influence in microstructural alterations and mechanical properties of 304 stainless steel weld joints. Journal of Engineering Science and Technology. 2023 July (18): 33–54.
12. Singh G, Mehta A, Vasudev H. Sustainability of additive manufacturing: a comprehensive review. Progress in Additive Manufacturing. 2024 Mar 21; 1–24.
13. Shiaa WQ, Abdulghafour AB, Hassoon OH. An enhanced technique for removing soft tissues and highlighting regions of interest in medical images. In AIP Conference Proceedings 2024 Jun 10; 3002(1). AIP Publishing.
14. Valvez S, Silva AP, Reis PN. Compressive behaviour of 3D-printed PETG composites. Aerospace. 2022 Feb 28; 9(3): 124.
15. Gibson I, Rosen DW, Stucker B, Khorasani M, Rosen D, Stucker B, Khorasani M. Additive manufacturing technologies. Cham, Switzerland: Springer; 2021.
16. Hassan MH, Omar AM, Daskalakis E, Hou Y, Huang B, Strashnov I, Grieve BD, Bártolo P. The potential of polyethylene terephthalate glycol as biomaterial for bone tissue engineering. Polymers. 2020 Dec 18; 12(12): 3045.
17. Petersmann S, Spoerk M, Van De Steene W, Üçal M, Wiener J, Pinter G, Arbeiter F. Mechanical properties of polymeric implant materials produced by extrusion-based additive manufacturing. Journal of the Mechanical Behavior of Biomedical Materials. 2020 Apr 1; 104: 103611.
18. Özen A, Auhl D, Völlmecke C, Kiendl J, Abali BE. Optimization of manufacturing parameters and tensile specimen geometry for fused deposition modeling (FDM) 3D-printed PETG. Materials. 2021 May 14; 14(10): 2556.
19. Mahesh V, Joseph AS, Mahesh V, Harursampath D, Vn C. Investigation on the mechanical properties of additively manufactured PETG composites reinforced with OMMT nanoclay and carbon fibers. Polymer Composites. 2021 May; 42(5): 2380–95.
20. Valvez S, Silva AP, Reis PN. Compressive behaviour of 3D-printed PETG composites. Aerospace. 2022 Feb 28; 9(3): 124.
21. Mohammed RN, Ganesh BK, Saminathan R. Flexural Modulus Enhancement and Minimization of Printing Time and Part Weight for PET-G, Using Taguchi-GRA-TOPSIS Techniques [J]. Materiale Plastice. 2022; 3.
22. Vijayasankar K.N., Falguni P. Effect of process parameters on the quality of Additively Manufactured PETG-Silk Composite. Applied Composite Materials. 2023 Feb; 30(1): 135–55.
23. Vijayakumar MD, Palaniyappan S, Veeman D, Tamilselvan M. Process optimization of hexagonally structured polyethylene terephthalate glycol and carbon fiber composite with added shell walls. Journal of Materials Engineering and Performance. 2023 Jul; 32(14): 6434–47.
24. Petousis M, Ntintakis I, David C, Sagris D, Nasikas NK, Korlos A, Moutsopoulou A, Vidakis N. A coherent assessment of the compressive strain rate response of PC, PETG, PMMA, and TPU thermoplastics in MEX additive manufacturing, Polymers 2023; 15(19).
25. Patil S, Sathish T, Giri J, Felemban BF. An experimental study of the impact of various infill parameters on the compressive strength of 3D printed PETG/CF. AIP Advances. 2024 Sep 1; 14(9).
26. Khudhir WS, Ahmed BA, Shukur JJ. Experimental investigation and optimization of surface roughness and kerf width in wire-EDM process. InAIP Conference Proceedings 2024 Jun 10; 3002(1). AIP Publishing.
27. Abdulridha HH, Abbas TF, Bedan AS. Predicting mechanical strength and optimized parameters in FDM-printed polylactic acid parts via artificial neural networks and desirability analysis. Management Systems in Production Engineering. 2024 Aug 1; 32(3).